Coupling Dynamics Analysis of the Flying Cable Driven Parallel Robot

Qin Wang, Hua Chen, Yu Su and Lu Qiao

***Abstract*—**Flying cable driven parallel robots consist of two subsystems, i.e. four-rotor unmanned aerial vehicle (QUV) and cable driven parallel robot (CDPR), which cooperate each other to complete various operations. Due to the cable flexibility, wind disturbance and base motion of QUV, the dynamics coupling exists between the two subsystems, leading to the imprecise dynamics modeling and cable tension determination. To describe the dynamics coupling, base motions of QUV can be viewed as the external disturbance and the motion of the cable can be decomposed of two categories: steady winding motion and vibration with small amplitude. Based on the space discretization of the cable, cable tension increment caused by vibration with small amplitude can be applied to describe the dynamics coupling. Thus, the cable tension can be determined precisely. Simulation results show that the cable vibration with small amplitude and base motion of QUV can affect the cable tension determination apparently, which should be take into account fully, thus providing the theoretical foundation for controlling the CDPR more accurately.

***Keywords*—**Dynamic coupling, Cable tension, Determination, flying robot, Vibration with small amplitude.

I. INTRODUCTION

THE cable driven parallel robot has the advantages of small inertia of the movement branch chain, high unit mass loading ratio, large workspace and simple structure, because of using cable as transmission element. But as one end of the cable is connected to the fixed pulley point, the working space is confined to a fixed area. If the workspace is wide, such as oil transmission or electricity transmission lines, mountains, fields, jungle or sea surface, the traditional base fixed cable traction parallel robot is not competent. With the help of the technology of UAV, the four-rotor unmanned aerial vehicle is used as the generalized base of the cable driven parallel robot, and a 6 degree of freedom cable driven parallel robot is suspended below it, and the flying cable driven parallel robot is formed. The combination of the four rotor UAV with cable driven parallel robot, on the one hand, to overcome the traditional "fixed base" type of cable driven parallel robot by terrain and landform factors have the disadvantages of large capacity range of movement can be performed such as disaster monitoring, high-rise fire, pipeline inspection, field survey, express transportation and other tasks on the other hand; lightweight cable can be alleviated to some extent the four rotor UAV endurance ability is weak, the bearing capacity of the weak. In addition, as a transmission element, the cables offer the simple structure, small upwind surface, uneasy interference and low cost.

At present, the research on flying cable driven parallel robots at home and abroad is still very few, basically staying in the exploration phase. Helicopter cable haulage is relatively mature, because of the similar structure, it can provide a reference for the research of flying cables towing robots. LUCASSAN and other established a three-degree-of-freedom helicopter suspended load suspension in the mathematical model and studied the dynamics at this time [2]. NONNENMACHER and other developed a helicopter hanger transport automatic stability and positioning system "HALAS", and conducted a flight test to verify the effectiveness of the system for the vibration suppression [3-5]. ADAMS and other input shaping combined with model follow-up control to reduce the hanging load swing [6] and build a test bed to verify the dynamic model and control effects [6]. However, all of these articles use a single-point to suspend the load. Therefore, "helicopter-cable-load" system is similar to a pendulum system, and the problem of load swing is prominent. OH and others propose using the "helicopter-cable driven parallel robot" system for water surface transportation [7], which effectively restrains the load swing and increases the complexity and control difficulty of the system. Although the influence of the helicopter base movement and wind disturbance on the moving platform are considered, the cable flexibility that leads to cable vibration with small amplitude are not taken into account. The flying cable driven robot proposed in this paper consists of two subsystems, a four-rotor UAV and a cable driven parallel robot. The two subsystems cooperate with each other to accomplish various operations. Due to the flexibility of the cables, however, there is a dynamic coupling between the two subsystems that must be taken into account. In this paper, the cable-dragged parallel robot is taken as the research object. The basic motion of the four-rotor UAV is taken as the disturbance, and the dynamic coupling between the two subsystems is described by the small vibration of the cable, so that the accurate dynamic model can be obtained.

This work was supported in part by Supported by NSFC (51705392). Shaanxi science and technology project(2016GY-175), Shaanxi provincial education office fund(17JK0361)

Qin Wang is with the School of Mechatronic Engineering, XI'AN technological University, Xi'an 710021, Shaanxi, China.

Hua Chen is with the School of Mechatronic Engineering, XI'AN technological University, Xi'an 710021, Shaanxi, China.

Yu Su is with the School of Mechatronic Engineering, XI'AN technological University, Xi'an 710021, Shaanxi, China. (corresponding author; e-mail: suyu@xatu.edu.cn).

II. Kinematic Analysis of a Cable Driven Parallel Robot

A. Establishment of kinematic model

Flying parallel robot structure as shown in Figure 1 flight type traction cable, cable tractive parallel robot suspended under the four rotor UAV, 6 pulling cables in the moving platform is suspended above the structure required by means of platform to realize the weight of force closure [8].

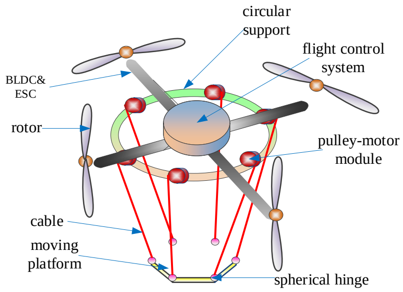

Fig. 1. Structure diagram of a flying cable driven parallel robot

The work of flying cable driven parallel robot requires the cooperation of two subsystems of four-rotor unmanned aerial vehicles and cable pulling parallel robots. Four-rotor UAVs provide a wide range of movement capabilities while cables control the moving platform for further fine motion. Therefore, in the kinematics analysis, the four-rotor UAV motion is taken as the basic motion to study the relationship between the pose and the cable length of the moving platform.

The establishment of a kinematic model of pedestal fixed cable-towed parallel robot requires only a global frame system fixed with the earth and a local frame system fixedly connected with the moving platform. However, two parallel moving robots exist simultaneously System, it is necessary to establish two local frame system to describe the system movement. As shown in picture 2, {G} is a global frame system fixed to the earth, O is the origin of frame system. X , Y , Z is the axis. The geographical east direction is the X axis, the north is the Y axis, Vertical upward direction for the Z axis. Established a local frame system {A} fixedly attached to the center of gravity of the four-rotor UAV. O_A is the origin of the frame system, and x_A, y_A, and z_A are frame axes. $\boldsymbol{x}_A$ is the position vector of O_A in {G}. ${}^G\boldsymbol{R}_A$ is a rotation transformation matrix from {A} to {G} in the form of

$$
{}^G\boldsymbol{R}_A=\begin{bmatrix} C\theta_a C\varphi_a & S\phi_a S\theta_a C\varphi_a - C\phi_a S\varphi_a & C\phi_a S\theta_a C\varphi_a + S\phi_a S\varphi_a \\ C\theta_a C\varphi_a & S\phi_a S\theta_a C\varphi_a + C\phi_a S\varphi_a & C\phi_a S\theta_a C\varphi_a - S\phi_a S\varphi_a \\ -S\theta_a & S\phi_a C\varphi_a & C\phi_a S\varphi_a \end{bmatrix} \tag{1}
$$

Where C and S represent the cos and sin functions, respectively; and ϕ_A, θ_A *and* φ_A represent the roll, pitch and yaw angles of the Four-rotor UAV about the x_A, y_A and z_A axes respectively in {A}.

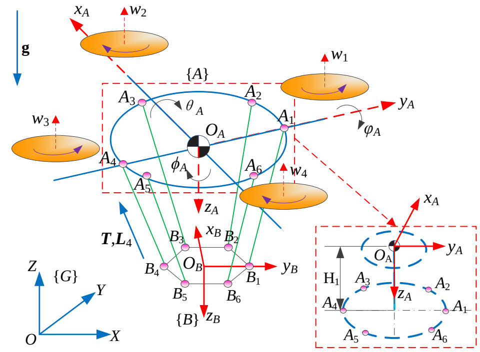

Fig. 2. Kinematic model of a flying cable driven parallel robot

Let A_i (i=1,2,…,6) be the hinge point between the cable and the pulley on the annular support, and $\boldsymbol{a}_i$ be the position vector in A_i at {A}. Let H_1 be the vertical distance from O_A to the torus support, with the A_i distribution angle α_A=60° and the radius of the distribution circle is r_A, then the position vector ${}^G\boldsymbol{A}_i$ of A_i in {G} is of the form:

$$
{}^G\boldsymbol{A}_i={}^G\boldsymbol{R}_A\boldsymbol{a}_i+\boldsymbol{x}_A \tag{2}
$$

where $\boldsymbol{a}_i$=[$r_A\cos((i\text{-}1)\alpha_A)$ $r_A\sin((i\text{-}1)\alpha_A)$ H_1]^T.

The local frame system {B}, which is fixedly connected to the center of gravity O_B of the moving platform, is established. O_B is the rotation transformation matrix with the frame origin, x_B, y_B and z_B as the frame axes and ${}^A\boldsymbol{R}_B$ is a rotation transformation matrix from {B} to {A} in the form:

$$
{}^A\boldsymbol{R}_B=\begin{bmatrix} C\theta_b C\varphi_b & S\phi_b S\theta_b C\varphi_b - C\phi_b S\varphi_b & C\phi_b S\theta_b C\varphi_b + S\phi_b S\varphi_b \\ C\theta_b C\varphi_b & S\phi_b S\theta_b C\varphi_b + C\phi_b S\varphi_b & C\phi_b S\theta_b C\varphi_b - S\phi_b S\varphi_b \\ -S\theta_b & S\phi_b C\varphi_b & C\phi_b S\varphi_b \end{bmatrix} \tag{2}
$$

Where ϕ_b, θ_b *and* φ_b are the roll, pitch and yaw angles of the moving platform about the x_B, y_B, z_B axes in {B}, respectively. $\boldsymbol{x}_b$ is the position vector of O_B in {A}. Let B_i (i=1, 2, …,6) be the hinge point between the cable and the moving platform, $\boldsymbol{b}_i$ is the position vector of B_i in {B}; H_2 is the vertical distance from O_B to the moving platform, and the distribution angle of B_i is α_B=60° and the radius of the distribution circle is r_B, then the position vector ${}^G\boldsymbol{B}_i$ of B_i in {G} is:

$$
{}^G\boldsymbol{B}_i={}^G\boldsymbol{R}_A\boldsymbol{x}_b+{}^G\boldsymbol{R}_A{}^A\boldsymbol{R}_B\boldsymbol{b}_i+\boldsymbol{x}_A \tag{3}
$$

In the formula, $\boldsymbol{b}_i$=[$r_B\cos((i\text{-}1)\alpha_A)$ $r_B\sin((i\text{-}1)\alpha_A)$ H_2]^T.

B. Cable length calculation

When parallel flying cable traction robot works, it has a limited range of cables, and the cable span height is relatively small, and the weight of the cable is very small. The cable sag is very small, and the shape of the cable can be seen as a straight line. So the length vector of the cable length [9] can be defined by the line segment between the cord end point A_i and the B_i:

$$
\boldsymbol{L}_i={}^G\boldsymbol{A}_i-{}^G\boldsymbol{B}_i={}^G\boldsymbol{R}_A\left(\boldsymbol{a}_i-\boldsymbol{x}_b-{}^A\boldsymbol{R}_B\boldsymbol{b}_i\right) \tag{4}
$$

Then the length of the cable can be obtained by the lower calculation:

$$
l_i=\left\|{}^o\boldsymbol{R}_A\left(\boldsymbol{a}_i-\boldsymbol{x}_b-{}^A\boldsymbol{R}_B\boldsymbol{b}_i\right)\right\|_2 \tag{5}
$$

From (6) we can see that the length of the cable has nothing to do with the position of the Four-rotor UAV, but with its posture and the position and posture of the moving platform. Given the attitude of the Four-rotor UAV, given one of the position or attitude of the moving platform, another variable can be controlled by changing the cable length. At the same time, we can see from (6) that the length of cables has nothing to do with the force, which is the ideal length after determining the trajectory of moving platform. But in fact, due to the flexibility of the cable, the cable will have a elastic elongation.

$$l_e = Fl/(EA) \tag{6}$$

Where F is cable tension, due to unilateral cable tension characteristics, need to maintain F>0. E is the elastic modulus of the cable, A is the cable cross-sectional area. However, in practical applications, the E level is about 100 GPa due to the use of high elastic modulus cables. Therefore, $Fl/EA\rightarrow 0$, we can ignore the cable elastic elongation.

III. Solving the Tension When the Cable Is Slightly Vibrated.

A. Two types of cable movement

From (6) we can see through the cable winding could control the space movement of platform. Ideally, moving platform in any position should be maintained at equilibrium. But in fact, due to the low stiffness of the cable and the small damping characteristics, there is a dynamic coupling between the four-rotor unmanned aerial vehicle and the cable-towed parallel robot. The basic motions and wind disturbances of the Four-rotor unmanned aerial vehicles will cause the moving platform to make low-frequency and slow-decay vibration near the equilibrium position. Conversely, the vibration of the moving platform will also cause the vibration of the cables and thus the four-rotor UAV motion.

At any moment t, the cable's movement can be regarded as a superposition of large-scale winding movement and small-amplitude low-frequency vibration. The corresponding tension at the cable end also includes the active traction tension during winding movement and the tension generated by small vibration Increment. According to the literature [10-12], the vibration of the cable is dominated by the longitudinal vibration along the cable direction. The vibration of the other two directions is negligible. Therefore, only the longitudinal vibration of the cable is considered in this paper. Cable winding movement by the pulley-motor module to provide traction through the motor to keep the cable tensioned and generated in the cable end of the traction tension $\boldsymbol{T}$, drag the mobile platform motion, balance dynamic platform external force; small vibration cable from the cable Low stiffness and small damping characteristics in the wind disturbance, four-rotor UAV basic movement makes the cable end of the small displacement offset position balance, the cable length also changes; at the same time the cable tension also changes, resulting in passive Tension increment $\Delta\boldsymbol{T}$, can be used to describe the dynamic coupling between the two subsystems, so cable tension F can be expressed as

$$\boldsymbol{F} = \boldsymbol{T} + \Delta\boldsymbol{T} \tag{7}$$

According to the general equations of dynamics, when the cable is slightly vibrated, the cable tension increment is: $\Delta\boldsymbol{T}=\Delta\boldsymbol{T}_M+\Delta\boldsymbol{T}_C+\Delta\boldsymbol{T}_K$, T_M is the inertial force, T_K is the elastic force, T_C is the damping force. Since the weight of the cable is ignored in this paper, the increment of the inertial force of cable motion, $\Delta\boldsymbol{T}_M=0$, so $\Delta\boldsymbol{T}=\Delta\boldsymbol{T}_C+\Delta\boldsymbol{T}_K$.

B. Damping force increment (ΔT_C) deduction

Cable winding movement by the motor controllable traction control for steady-state movement. On this basis, the cable vibrates slightly, and the spatial position of the cable end point B_i becomes

$${}^G\boldsymbol{B}_{new} = {}^G\boldsymbol{B} + \Delta\boldsymbol{B} \tag{8}$$

Where $\Delta\boldsymbol{B}$ is the displacement increment of B_i relative to steady-state motion ${}^G\boldsymbol{B}$. The micro-pose change of the moving platform can be precisely measured by the measuring device, it's: $\Delta\boldsymbol{X}=[\Delta\boldsymbol{x}_B\ \Delta\boldsymbol{\Theta}_B]^T$ in {G}, where $\Delta\boldsymbol{x}_B=[\Delta x_B\ \Delta y_B\ \Delta z_B]^T$, $\Delta\boldsymbol{\Theta}_B=[\Delta\phi_B\ \Delta\theta_B\ \Delta\varphi_B]^T$, sampling time is Δt. Notice that for a small amount μ, $\sin\mu=0$, $\cos\mu=1$, $\mu=\Delta\phi_B$, $\Delta\theta_B$, $\Delta\varphi_B$, so the frame square matrix ($\Delta\bar{\boldsymbol{\Theta}}_B$) of the vector $\Delta\boldsymbol{\Theta}_B$ can be obtained:

$$\Delta\bar{\boldsymbol{\Theta}}_B = \begin{bmatrix} 0 & -\Delta\varphi & \Delta\theta \\ \Delta\varphi & 0 & -\Delta\phi \\ -\Delta\theta & \Delta\phi & 0 \end{bmatrix} \tag{9}$$

Then we could obtain $\Delta\boldsymbol{B}$ from the formula below:

$$\Delta\boldsymbol{B} = \Delta\boldsymbol{x}_B + \Delta\bar{\boldsymbol{\Theta}}_B\left({}^G\boldsymbol{R}_A{}^A\boldsymbol{R}_B\boldsymbol{b}\right) \tag{10}$$

Let C be the cable damping factor, then the damping force recrement at the cable end B_i in {G} is:

$$\Delta T_C = C\Delta\dot{\tilde{l}} = C\frac{l\left({}^G\boldsymbol{B}_{new}\right) - l\left({}^G\boldsymbol{B}\right)}{\Delta t} \tag{11}$$

Where $\Delta\tilde{l}$ is the cable length changes caused by cable's small vibration.

C. Deduction of elastic force increment ΔT_K

Cable winding movement can be regarded as a whole cable as a straight line, its essence is no mass two lever unit. Can only describe one-way force characteristics of the cable cannot reflect the flexibility and damping characteristics of the cable. The study of the elastic force generated when the cable vibrates cannot directly use the whole unit, but need finite element method to discretize the cable [13-15], the cable is divided into several small linear units. As shown in Figure 3, each cable is discretized into n units. Node 1 is connected to a pulley mounted on a toroidal support, and node n+1 is connected to a moving platform. All elements have the same length, $e=l(t)/n$, where $l(t)$ is the cable length at time t and $l(t)$ changes with time. The local frame system of cable {c} is established. o_c is the origin of frames located at node 1 and x_c is along the axis of cable. Take one of the tiny units j , j=1,2,…,n. Element j is subjected to tension τ at its nodes j-1 and j, which are the same size and opposite in direction of x_c due to the neglect of cable quality. The positions of nodes j-1 and j on the x_c axis are x_c^{j-1} and x_c^j respectively.

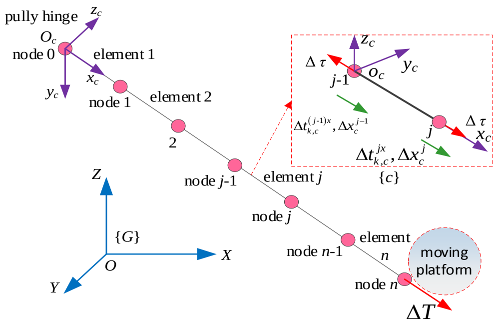

Fig. 3. Cable discretization model

In a small period interval Δt, the cable movement can be seen as a steady state winding movement and a slight vibration superimposed. The steady-state winding movement causes the cable length change while the number of units n is constant, so dose the unit length. The minor vibration of the cable causes slight displacement of the cable in the axial direction, resulting in the discrete nodes on the cable deviating from the equilibrium position. Both movements of the cable lead to an increase in tension $\Delta\tau$. $\Delta\tau$ and node position offset and the relationship between the length of the unit as shown in the following formula

$$\Delta\tau = \frac{EA}{e}\left(\Delta x_c^j - \Delta x_c^{j\text{-}1}\right) + \frac{EA}{e}\Delta e \tag{12}$$

In the formula, Δe is the increment of unit length due to the change of cable length caused by the retraction of the cable, $\Delta e=[l(t+\Delta t)-l(t)]/n$; and the node force increment Δx_c^j of node j-1 and j-1 in {c} can be calculated by the following formula:

$$\begin{cases} \Delta t_{k,c}^{(j\text{-}1)x} = \Delta\tau = \dfrac{EA}{e}\left(\Delta x_c^{j\text{-}1} - \Delta x_c^j - \Delta e\right) \\ \Delta t_{k,c}^{jx} = -\Delta\tau = \dfrac{EA}{e}\left(-\Delta x_c^{j\text{-}1} + \Delta x_c^j + \Delta e\right) \end{cases} \tag{13}$$

Equation (14) can be further written in matrix form：

$$\Delta \boldsymbol{t}_{k,c}^j = \boldsymbol{k}_{n,c}^j \Delta \boldsymbol{x}_c^j + \boldsymbol{k}_{l,c}^j \Delta \boldsymbol{e}_c^j \tag{14}$$

where $\Delta \boldsymbol{t}_{k,c}^j = \left[\Delta t_{k,c}^{(j\text{-}1)x} \quad \Delta t_{k,c}^{jx}\right]^T$, $\Delta \boldsymbol{e}_c^j = \left[\Delta e \quad \Delta e\right]^T$, $\Delta \boldsymbol{x}_c^j = \left[\Delta x_c^{j-1} \quad \Delta x_c^j\right]^T$ is the node offset in {c}, and:

$$\boldsymbol{k}_{n,c}^j = \frac{EA\operatorname{sgn}(j)}{e}\begin{bmatrix} 1 & -1 \\ -1 & 1 \end{bmatrix}, \quad \boldsymbol{k}_c^l = \frac{EA\operatorname{sgn}(i)}{\Delta e}\begin{bmatrix} 1 \\ -1 \end{bmatrix} \tag{15}$$

In which:

$$\operatorname{sgn}(j) = \begin{cases} 1 & \Delta x_c^{j\text{-}1} \wedge \Delta x_c^j > 0 \\ 0 & \Delta x_c^{j\text{-}1} \wedge \Delta x_c^j \le 0 \end{cases} \tag{16}$$

When $\Delta x_c^{j\text{-}1} \wedge \Delta x_c^j > 0$, the node offset direction points to the node j, the cable is subjected to the pulling force, so sgn(j)=1; when $\Delta x_c^{j\text{-}1} \wedge \Delta x_c^j = 0$, the node without offset or minor vibration, indicating that the cable is unstressed, so sgn(j)=0; when $\Delta x_c^{j\text{-}1} \wedge \Delta x_c^j > 0$, node offset direction points to node j-1, the cable is compressed, which is contradictory with the fact that the cable can not bear the pressure, the cable will be unstable, so sgn(j)=0. EA/e represents the unit stiffness coefficient, once the cable material is determined, E and A fixed, the unit stiffness coefficient and unit length only. When the number of units is fixed, the unit stiffness decreases when the cable length increases and the unit stiffness increases when the cable length decreases. It should be noted that $\Delta \boldsymbol{t}_{k,c}$ is the unit node force increment in the cable local frame system {c}, and the overall system dynamics analysis needs to be performed in the global frame system. Therefore, we need to convert $\Delta \boldsymbol{t}_{k,c}$ from {c} to {G} by rotating the transformation matrix. Reference [10], the rotation transformation matrix ${}^G\boldsymbol{R}_c$ is obtained as follows

$${}^G\boldsymbol{R}_c = \begin{bmatrix} \boldsymbol{u}_{1\times3}^T & \boldsymbol{0}_{1\times3} \\ \boldsymbol{0}_{1\times3} & \boldsymbol{u}_{1\times3}^T \end{bmatrix}_{2\times6} \tag{17}$$

where $\boldsymbol{u}^T = \boldsymbol{L}(t)^T / l(t) = \begin{bmatrix} u_x & u_y & u_z \end{bmatrix}$, $\boldsymbol{0}_{3\times1}$=[0 0 0]。So in {G}, $\boldsymbol{k}_{n,c}^j$, $\boldsymbol{k}_{l,c}^j$,$\Delta \boldsymbol{x}_c^j$ and $\Delta \boldsymbol{e}_c^j$ are transferred to

$$\begin{aligned} \boldsymbol{k}_n^j &= {}^G\boldsymbol{R}_c^T \boldsymbol{k}_{n,c}^j \, {}^G\boldsymbol{R}_c = \left[\begin{array}{c|c} \boldsymbol{k}_1 & \boldsymbol{k}_2 \\ \hline \boldsymbol{k}_3 & \boldsymbol{k}_4 \end{array}\right]_{6\times6} \\ \boldsymbol{k}_l^j &= {}^G\boldsymbol{R}_c^T \boldsymbol{k}_{l,c}^j = \begin{bmatrix} \boldsymbol{k}_5 & \boldsymbol{k}_6 \end{bmatrix}_{6\times1}^T \\ \Delta \boldsymbol{x}^j &= {}^G\boldsymbol{R}_c^T \Delta \boldsymbol{x}_c^j = \left[\Delta x_c^{j-1}\boldsymbol{u} \quad \Delta x_c^j \boldsymbol{u}\right]_{6\times1}^T \\ \Delta \boldsymbol{e}^j &= {}^G\boldsymbol{R}_c^T \Delta \boldsymbol{e}_c^j = \left[\Delta e^{j-1}\boldsymbol{u} \quad \Delta e^j \boldsymbol{u}\right]_{6\times1}^T \end{aligned} \tag{18}$$

In the formula, $\boldsymbol{k}_5$=-$S(j)\boldsymbol{u}$, $\boldsymbol{k}_6$=$S(j)\boldsymbol{u}$, $S(j)$=EAsgn(j)/e。$\boldsymbol{k}_1$, $\boldsymbol{k}_2$, $\boldsymbol{k}_3$, $\boldsymbol{k}_4$ shows below:

$$k_1 = S(j)\begin{bmatrix} u_x^2 & u_x u_y & u_x u_z \\ u_y u_x & u_y^2 & u_y u_z \\ u_z u_x & u_z u_y & u_z^2 \end{bmatrix}, \quad k_2 = S(j)\begin{bmatrix} -u_x^2 & -u_x u_y & -u_x u_z \\ -u_y u_x & -u_y^2 & -u_y u_z \\ -u_z u_x & -u_z u_y & -u_z^2 \end{bmatrix} \tag{19}$$

Then

$$\Delta \boldsymbol{t}_k^j = \boldsymbol{k}_n^j \Delta \boldsymbol{x}^j + \boldsymbol{k}_l^j \Delta \boldsymbol{e}^j \tag{20}$$

where $\Delta \boldsymbol{t}_k^j = \left[\Delta \boldsymbol{t}_k^{(j-1)x} \quad \Delta \boldsymbol{t}_k^{jx}\right]^T$. The elastic force $\Delta\Sigma\boldsymbol{T}_K$ of the whole cable can be obtained by the finite element operation of (15):

$$\Delta\Sigma\boldsymbol{T}_K = \sum_j \boldsymbol{k}_n^j \Delta \boldsymbol{x}^j + \sum_j \boldsymbol{k}_l^j \Delta \boldsymbol{e}^j = \boldsymbol{K}_n \Delta \boldsymbol{X} + \boldsymbol{K}_l \Delta \boldsymbol{E} \tag{21}$$

In the formula, $\sum$ is a finite element assembly operator, and the assembly process of the total stiffness matrix $\boldsymbol{K}_c$ and $\boldsymbol{K}_l$ is shown in Figure 4. $\boldsymbol{K}_n$ is 3 (n+1) order matrix, $\boldsymbol{K}_l$ is 3(n+1) vectors. $\Delta \boldsymbol{X} = \underbrace{\left[\Delta x_c^0 \boldsymbol{u} \quad \Delta x_c^1 \boldsymbol{u} \quad \cdots \quad \Delta x_c^n \boldsymbol{u} \right]^T}_{n+1}$ is a 3 (n + 1) -dimensional column vector composed of node displacement offset vectors , $\Delta \boldsymbol{E} = \underbrace{\left[\Delta e^0 \boldsymbol{u} \quad \Delta e^1 \boldsymbol{u} \quad \cdots \quad \Delta e^n \boldsymbol{u} \right]^T}_{n+1}$ is a 3 (n + 1) -dimensional column vector composed of unit length increment vectors, so: $\Delta \Sigma \boldsymbol{T_K} = \underbrace{\left[\Delta \boldsymbol{t}_k^{0x} \quad \Delta \boldsymbol{t}_k^{1x} \quad \cdots \quad \Delta \boldsymbol{t}_k^{nx} \right]^T}_{n+1}$ is a 3 (n + 1) dimensional column vector, the elastic force at the end point B_i of the cable is $\Delta \boldsymbol{T_K} = \Delta \boldsymbol{t}_k^{nx}$, The size of the value is $\Delta T_K = \left\| \Delta \boldsymbol{t}_k^{nx} \right\|_2$

(22)

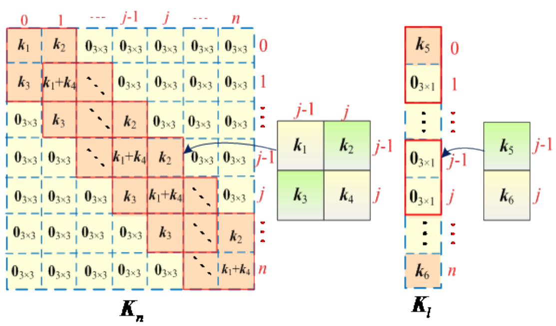

Fig. 4. Cable local frame system total stiffness matrix assembly process

At this point, the cable end tension in the small amplitude vibration of the cable is obtained as:

$$\Delta \boldsymbol{T} = \Delta \boldsymbol{T_K} + \Delta \boldsymbol{T_C} \tag{23}$$

It is necessary to point out that for the convenience of writing, the numbered subscript (i) of the cable is omitted in the deduction of this section (i=1,2,……n+1) , In fact, the derivation of this section is established for every cable deduction. According to (24) the tension of the tension vector can be obtained by the 2 norm of the tension vector (ΔT_i) , the tension size of the cable i can be obtained, and the direction is directed from B_i to A_i.

IV. Dynamic Analysis of a Parallel Cable Traction Robot

A. Force balance of a cable traction parallel robot

The motion of the four rotor UAV will affect the motion of the cable driven parallel robot. In this paper, the basic motion of the four rotor UAV is regarded as disturbance, and the cable driven parallel robot is taken as the research object. The force balance equation is set up at the center of gravity of the moving platform O_B.

$$m_B \frac{\mathrm{d}^2 \boldsymbol{x}_B}{\mathrm{d}t^2} = m_B \mathbf{g} + \left[\boldsymbol{u}_1 \quad \boldsymbol{u}_2 \quad \cdots \quad \boldsymbol{u}_6 \right]_{3\times6} \left(\boldsymbol{T} + \Delta \boldsymbol{T} \right) + \boldsymbol{F}_e \tag{24}$$

$\boldsymbol{F}_e$ is the wind disturbance acting on the moving platform, $\boldsymbol{F}_e=[F_{ex}\ F_{ey}\ F_{ez}]^T$, could be obtained by formulas below:

$$F_{ex} = \frac{1}{2} C_d \rho V_{wx}^2 S$$
$$F_{ey} = \frac{1}{2} C_d \rho V_{wy}^2 S$$
$$F_{ez} = \frac{1}{2} C_l \rho \left(V_{wx}^2 + V_{wy}^2 \right) S \tag{25}$$

In the formulas, $V_w=[V_{wx}\ V_{wy}\ V_{wz}]^T$, C_d is resistance coefficient , C_l is lift coefficient , S is the maximum cross section area of moving platform。 m_B is the quality of the dynamic platform , $\boldsymbol{u}_i = \boldsymbol{L}_i / l_i$ 。 $\boldsymbol{T}=[T_1\ T_2 \ldots T_6]^T$ is the tension vector of the cable end at the steady state of 6 cables , also is the driving force of the motor output ; $\Delta\boldsymbol{T}=[\Delta T_1\ \Delta T_2 \ldots \Delta T_6]$ is the increment vector of cable end tension during small amplitude vibration。 $\boldsymbol{x}_B$ is the position vector of O_B in {G} , $\boldsymbol{x}_B = (\boldsymbol{x}_A + {}^G\boldsymbol{R}_A \boldsymbol{x}_b)$, take them to the formula (25):

$$m_B \ddot{\boldsymbol{x}}_b + \overbrace{m_B {}^G\boldsymbol{R}_A^T (\ddot{\boldsymbol{x}}_A + {}^G\ddot{\boldsymbol{R}}_A \boldsymbol{x}_b + 2\,{}^G\dot{\boldsymbol{R}}_A \dot{\boldsymbol{x}}_b) - {}^G\boldsymbol{R}_A^T m_B \mathbf{g}}^{\boldsymbol{D}_{F,b}} - \left[\boldsymbol{u}_1 \quad \boldsymbol{u}_2 \quad \cdots \quad \boldsymbol{u}_6 \right]_{3\times6} \Delta \boldsymbol{T} - \boldsymbol{F}_e = \left[\boldsymbol{u}_1 \quad \boldsymbol{u}_2 \quad \cdots \quad \boldsymbol{u}_6 \right]_{3\times6} \boldsymbol{T} \tag{26}$$

In the (27) formula, we will define $\boldsymbol{x}_A$ and ${}^G\boldsymbol{R}_A$----the motion related to the four rotor unmanned aerial vehicle, that is, xA and GRA as the interference term $\boldsymbol{D}_{F,B}$. It describes the force acting on the moving platform by the four rotor UAV.

B. Parallel cable-driven robot torque balance

Quadractorial UAV position vector in $\{A\}$ is: $\boldsymbol{X}_a=[\boldsymbol{x}_a\ \boldsymbol{\Theta}_a]^T=[x_a\ \ y_a\ \ z_a\ \ \phi_a\ \ \theta_a\ \ \varphi_a]^T$, angular velocity is: $\dot{\boldsymbol{\Theta}}_a = \left[\dot{\phi}_a \quad \dot{\theta}_a \quad \dot{\varphi}_a \right]^T$. The angular velocity ${}^A\boldsymbol{\omega}_{AG}$ of {A} relative to {G} in {A} can be defined as

$${}^A\boldsymbol{\omega}_{AG} = \begin{bmatrix} \omega_{ax} \\ \omega_{ay} \\ \omega_{az} \end{bmatrix} = \begin{bmatrix} 1 & 0 & -S\theta_a \\ 0 & C\phi_a & S\phi_a C\theta_a \\ 0 & -S\phi_a & C\phi_a C\theta_a \end{bmatrix} \begin{bmatrix} \dot{\phi}_a \\ \dot{\theta}_a \\ \dot{\varphi}_a \end{bmatrix} = \boldsymbol{P}_a \dot{\boldsymbol{\Theta}}_a \tag{27}$$

The position vector of the moving platform in {B} is: $\boldsymbol{X}_b=[\boldsymbol{x}_b\ \boldsymbol{\Theta}_b]^T=[x_b\ y_b\ z_b\ \phi_b\ \theta_b\ \varphi_b]^T$, angular velocity is $\dot{\boldsymbol{\Theta}}_b = \left[\dot{\phi}_b \quad \dot{\theta}_b \quad \dot{\varphi}_b \right]^T$. In {B}, the angular velocity ${}^B\boldsymbol{\omega}_{BA}$ of {B} relative to {A} can be defined as

$${}^B\boldsymbol{\omega}_{BA} = \begin{bmatrix} \omega_{bx} \\ \omega_{by} \\ \omega_{bz} \end{bmatrix} = \begin{bmatrix} 1 & 0 & -S\theta_b \\ 0 & C\psi_b & S\psi_b C\theta_b \\ 0 & -S\psi_b & C\psi_b C\theta_b \end{bmatrix} \begin{bmatrix} \dot{\phi}_b \\ \dot{\theta}_b \\ \dot{\varphi}_b \end{bmatrix} = \boldsymbol{P}_b \dot{\boldsymbol{\Theta}}_b \tag{28}$$

Similar to the force balance, the four-rotor unmanned aerial vehicle (UAV) is used as the external disturbance, and the parallel cable-driven robot is taken as the research object. Establish the moment equilibrium equation at the moving platform center of gravity O_B.

$$\boldsymbol{I}_B{}^G\boldsymbol{\alpha}_{BO}+{}^G\boldsymbol{\omega}_{BO}\times\boldsymbol{I}_B{}^G\boldsymbol{\omega}_{BO}=\left[\boldsymbol{r}_{B1}\times\boldsymbol{u}_1\cdots\boldsymbol{r}_{B6}\times\boldsymbol{u}_6\right]_{3\times6}\left(\boldsymbol{T}+\Delta\boldsymbol{T}\right)+\boldsymbol{M}_e \tag{29}$$

Where $\boldsymbol{I}_B$ is the inertia matrix in {G} of the moving platform and $\boldsymbol{I}_B={}^G\boldsymbol{R}_B\boldsymbol{I}_b{}^G\boldsymbol{R}_B^T={}^o\boldsymbol{R}_A{}^A\boldsymbol{R}_B\boldsymbol{I}_b\left({}^G\boldsymbol{R}_A{}^A\boldsymbol{R}_B\right)^T$, $\boldsymbol{I}_b$ is the inertia of the moving platform in {B} ; $\boldsymbol{r}_{B,i}$ is the position vector of Bi in {G} , $\boldsymbol{r}_{B,i}={}^G\boldsymbol{R}_B\boldsymbol{b}_i={}^G\boldsymbol{R}_A{}^A\boldsymbol{R}_B\boldsymbol{b}_i$, i=1,2,……6 ; $\boldsymbol{M}_e$ is acting on the moving platform wind disturbance torque. Since the frame system is built on the center of gravity of the moving platform, the wind disturbance torque is 0. ${}^o\boldsymbol{\alpha}_{BO}$ is the angular acceleration of {B} for {G}. Due to ${}^G\boldsymbol{\omega}_{BG}={}^G\boldsymbol{\omega}_{AG}+{}^G\boldsymbol{\omega}_{BA}={}^G\boldsymbol{R}_A{}^A\boldsymbol{\omega}_{AG}+{}^G\boldsymbol{R}_A{}^A\boldsymbol{R}_B{}^B\boldsymbol{\omega}_{BA}$, we could get:

$$\begin{aligned}{}^G\boldsymbol{\alpha}_B&=\frac{\mathrm{d}}{\mathrm{d}t}{}^G\boldsymbol{\omega}_B=\frac{\mathrm{d}}{\mathrm{d}t}\left[{}^G\boldsymbol{R}_A{}^A\boldsymbol{\omega}_{AG}+{}^G\boldsymbol{R}_A{}^A\boldsymbol{R}_B{}^B\boldsymbol{\omega}_{BA}\right]=\\&{}^G\dot{\boldsymbol{R}}_A{}^A\boldsymbol{\omega}_{AG}+{}^G\boldsymbol{R}_A{}^A\dot{\boldsymbol{\omega}}_{AO}+{}^G\dot{\boldsymbol{R}}_B{}^B\boldsymbol{\omega}_{BA}+{}^G\boldsymbol{R}_A{}^A\boldsymbol{R}_B{}^B\dot{\boldsymbol{\omega}}_{BA}=\\&{}^G\boldsymbol{R}_A\left[{}^A\boldsymbol{\alpha}_{AG}+{}^A\boldsymbol{R}_B{}^B\boldsymbol{\alpha}_{BA}+\left({}^A\boldsymbol{\omega}_{AG}\times{}^A\boldsymbol{R}_B{}^B\boldsymbol{\omega}_{BA}\right)\right]\end{aligned} \tag{30}$$

Where ${}^A\boldsymbol{\alpha}_{AG}$ is the angular acceleration of {A} for {G} in {A}, and ${}^B\boldsymbol{\alpha}_{BA}$ is the angular acceleration of {B} relative to {G} in {B}, in the form of:

$${}^A\boldsymbol{\alpha}_A={}^A\dot{\boldsymbol{\omega}}_A=\left[\dot{\omega}_{a,x}\quad\dot{\omega}_{a,y}\quad\dot{\omega}_{a,z}\right]^T=\dot{\boldsymbol{P}}_a\dot{\boldsymbol{\Theta}}_a+\boldsymbol{P}_a\ddot{\boldsymbol{\Theta}}_a \tag{31}$$

$${}^B\boldsymbol{\alpha}_{BA}={}^B\dot{\boldsymbol{\omega}}_{BA}=\left[\dot{\omega}_{b,x}\quad\dot{\omega}_{b,y}\quad\dot{\omega}_{b,z}\right]^T=\dot{\boldsymbol{P}}_b\dot{\boldsymbol{\Theta}}_b+\boldsymbol{P}_b\ddot{\boldsymbol{\Theta}}_b \tag{32}$$

Bring (28), (29), (31), (32) and (33) into (30)

$$\begin{aligned}&{}^o\boldsymbol{R}_A\Big\{{}^A\boldsymbol{R}_B\boldsymbol{I}_b\left(\dot{\boldsymbol{P}}_b\dot{\boldsymbol{\Theta}}_b+\boldsymbol{P}_b\ddot{\boldsymbol{\Theta}}_b\right)+{}^A\boldsymbol{R}_B\boldsymbol{P}_b\dot{\boldsymbol{\Theta}}_b\times{}^A\boldsymbol{R}_B\boldsymbol{I}_b\boldsymbol{P}_b\dot{\boldsymbol{\Theta}}_b+\\&{}^A\boldsymbol{R}_B\boldsymbol{I}_b{}^A\boldsymbol{R}_B^T\left(\dot{\boldsymbol{P}}_a\dot{\boldsymbol{\Theta}}_a+\boldsymbol{P}_a\ddot{\boldsymbol{\Theta}}_a\right)+{}^A\boldsymbol{R}_B\boldsymbol{I}_b{}^A\boldsymbol{R}_B^T\left(\boldsymbol{P}_a\dot{\boldsymbol{\Theta}}_a\times{}^A\boldsymbol{R}_B\boldsymbol{P}_b\dot{\boldsymbol{\Theta}}_b\right)+\\&\left(\boldsymbol{P}_a\dot{\boldsymbol{\Theta}}_a+{}^AR_B\boldsymbol{P}_b\dot{\boldsymbol{\Theta}}_b\right)\times{}^A\boldsymbol{R}_B\boldsymbol{I}_b{}^A\boldsymbol{R}_B^T\boldsymbol{P}_a\dot{\boldsymbol{\Theta}}_a+\boldsymbol{P}_b\dot{\boldsymbol{\Theta}}_b\times{}^A\boldsymbol{R}_B\boldsymbol{I}_b\boldsymbol{P}_b\dot{\boldsymbol{\Theta}}_b\Big\}=\\&{}^o\boldsymbol{R}_A\left[{}^A\boldsymbol{R}_B\boldsymbol{b}_1\times\boldsymbol{u}_1\cdots{}^A\boldsymbol{R}_B\boldsymbol{b}_6\times\boldsymbol{u}_6\right]_{3\times6}\left(\boldsymbol{T}'+\boldsymbol{F}'\right)+\boldsymbol{M}_e\end{aligned} \tag{33}$$

(34) can be further grouping available

$$\begin{aligned}&{}^A\boldsymbol{R}_B\boldsymbol{I}_b\boldsymbol{P}_b\ddot{\boldsymbol{\Theta}}_b+\boldsymbol{F}_{O.b}+\boldsymbol{D}_{O.b}-{}^G\boldsymbol{R}_A\left[{}^A\boldsymbol{R}_B\boldsymbol{b}_1\times\boldsymbol{u}_1\cdots{}^A\boldsymbol{R}_B\boldsymbol{b}_6\times\boldsymbol{u}_6\right]_{3\times6}\Delta\boldsymbol{T}-{}^G\boldsymbol{R}_A^T\boldsymbol{M}_e\\&=\left[{}^A\boldsymbol{R}_B\boldsymbol{r}_{B1}\times\boldsymbol{u}_1\ldots{}^A\boldsymbol{R}_B\boldsymbol{r}_{B6}\times\boldsymbol{u}_6\right]\boldsymbol{T}\end{aligned} \tag{34}$$

Where

$$\boldsymbol{F}_{M.b}={}^A\boldsymbol{R}_B\boldsymbol{I}_b\dot{\boldsymbol{P}}_b\dot{\boldsymbol{\Theta}}_b+{}^A\boldsymbol{R}_B\boldsymbol{P}_b\dot{\boldsymbol{\Theta}}_b\times{}^A\boldsymbol{R}_B\boldsymbol{I}_b\boldsymbol{P}_b\dot{\boldsymbol{\Theta}}_b \tag{35}$$

$$\begin{aligned}\boldsymbol{D}_{M.b}=&{}^A\boldsymbol{R}_B\boldsymbol{I}_b{}^A\boldsymbol{R}_B^T(\dot{\boldsymbol{P}}_a\dot{\boldsymbol{\Theta}}_a+\boldsymbol{P}_a\ddot{\boldsymbol{\Theta}}_a)+\\&{}^A\boldsymbol{R}_B\boldsymbol{I}_b{}^A\boldsymbol{R}_B^T\left(\boldsymbol{P}_a\dot{\boldsymbol{\Theta}}_a\times{}^A\boldsymbol{R}_B\boldsymbol{P}_b\dot{\boldsymbol{\Theta}}_b\right)+\\&\left(\boldsymbol{P}_a\dot{\boldsymbol{\Theta}}_a+{}^A\boldsymbol{R}_B\boldsymbol{P}_b\dot{\boldsymbol{\Theta}}_b\right)\times{}^A\boldsymbol{R}_B\boldsymbol{I}_b{}^A\boldsymbol{R}_B^T\boldsymbol{P}_a\dot{\boldsymbol{\Theta}}_a+\\&\boldsymbol{P}_a\dot{\boldsymbol{\Theta}}_a\times{}^A\boldsymbol{R}_B\boldsymbol{I}_b\boldsymbol{P}_b\dot{\boldsymbol{\Theta}}_b\end{aligned} \tag{36}$$

C. Establishment of Dynamic Model of Parallel Cable-driven Robot

Combining (27) and (35), we get the kinetic equation

$$\begin{aligned}&\overbrace{\begin{bmatrix}m_b\boldsymbol{I}_3&\boldsymbol{0}_3\\\boldsymbol{0}_3&{}^A\boldsymbol{R}_B\boldsymbol{I}_b\boldsymbol{P}_b\end{bmatrix}}^{\boldsymbol{M}_B}\begin{bmatrix}\ddot{\boldsymbol{x}}_b\\\ddot{\boldsymbol{\Theta}}_b\end{bmatrix}+\overbrace{\begin{bmatrix}\boldsymbol{0}_{3\times1}\\\boldsymbol{F}_{M,b}\end{bmatrix}}^{\boldsymbol{F}_B}+\overbrace{\begin{bmatrix}\boldsymbol{D}_{F.b}\\\boldsymbol{D}_{M.b}\end{bmatrix}}^{\boldsymbol{D}_B}-\overbrace{\begin{bmatrix}\boldsymbol{F}_e\\\boldsymbol{M}_e\end{bmatrix}}^{\boldsymbol{W}_e}-\\&-\overbrace{\begin{bmatrix}\boldsymbol{u}_1&\cdots&\boldsymbol{u}_6\\{}^A\boldsymbol{R}_B\boldsymbol{r}_{B1}\times\boldsymbol{u}_1&\cdots&{}^A\boldsymbol{R}_B\boldsymbol{r}_{B6}\times\boldsymbol{u}_6\end{bmatrix}}^{\boldsymbol{J}}\Delta\boldsymbol{T}=\\&\overbrace{\begin{bmatrix}\boldsymbol{u}_1&\cdots&\boldsymbol{u}_6\\{}^A\boldsymbol{R}_B\boldsymbol{r}_{B1}\times\boldsymbol{u}_1&\cdots&{}^A\boldsymbol{R}_B\boldsymbol{r}_{B6}\times\boldsymbol{u}_6\end{bmatrix}}^{\boldsymbol{J}}\boldsymbol{T}\end{aligned} \tag{37}$$

In the formula, $\boldsymbol{I}_3$ is the third order unit matrix, $\boldsymbol{0}_3$ is the third order 0 matrix, (38) can be further simplified

$$\boldsymbol{M}_B\ddot{\boldsymbol{X}}_b+\boldsymbol{F}_B+\boldsymbol{D}_B-\boldsymbol{W}_e-\boldsymbol{J}\Delta\boldsymbol{T}=\boldsymbol{J}\boldsymbol{T} \tag{38}$$

In the formula, $\boldsymbol{D}_B$ is the disturbance of basic movement of four-rotor unmanned aerial vehicle to the cable-towed parallel robot; $\boldsymbol{W}_e$ is the wind disturbance; $\boldsymbol{J}$ is the structural matrix of the robot, which characterizes the direction of cable tension and tension moment. According to this formula can be calculated by the motor driving force, that is, traction tension.

V. The Process of solving the cable's driving force

In the second and third section, after calculating the small amplitude vibration of the cable and establishing the parallel robot dynamics model, we can calculate the driving force that the motor should output, that is cable tension.

1) The articulated points A_i and B_i (i=1, 2, ……, 6) of the given cables at the four rotor unmanned aerial vehicle and the moving platform. the distribution position, the small discrete time step length Δt, the elastic modulus E of the cable, the cross-section area A and the damping coefficient C;

2) At any instantaneous t=0, the position $\boldsymbol{X}_a(t)$ and $\boldsymbol{X}_b(t)$ of the four rotor unmanned aerial vehicle and the moving platform are calculated, and the cable length $l_i(t)$ is calculated by (6), and set k=0 .

3) Each cable i is divided into n units, and the unit length $e_i(t)=l_i(t)/n$

4) According to (11), the end of the cable is offset by a small amplitude vibration of ΔB, and then the increment (ΔT_C) of the end damping force of the cable is obtained by (12).

5) According to (23) the increment of the elastic force ΔT_K of the end end of the cable is obtained when the small amplitude vibration is obtained.

6) When the cable is under small vibration, the tension increment ΔT of the cable end is calculated from (24).

7) According to (39) calculate the cable end of the cable tension $\boldsymbol{T}(t)=\boldsymbol{J}^{-1}\left(\boldsymbol{M}_B\ddot{\boldsymbol{X}}_b(t)+\boldsymbol{F}_B+\boldsymbol{D}_B-\boldsymbol{W}_e-\boldsymbol{J}\boldsymbol{T}'(t)\right)$

8) Let k=k+1, then t=t+$k\Delta t$ and turn 2), repeat 2) -7) step until the end of the calculation of all the attitude and

attitude of the cable tension.

VI. Simulation Example

The simulation parameters of the fling cable driven parallel robot are shown in Table 1. The inertia array $\boldsymbol{I}_b$=diag(I_X, I_Y, I_Z) of the moving platform is the 3 order diagonal array. In order to simulate the fluctuating and intermittent characteristics of wind, wind disturbance is set as trapezoidal wave, the maximum wind speed in X direction is 5m/s, the maximum wind speed in Y direction is 6m/s, and Z to the maximum wind speed is 2m/s. In order to simulate the random characteristics of the wind, the Gauss random sequence is superimposed on the trapezoidal wave basis, the amplitude [-0.5, 0.5]m/s, and the final superposition results are shown in Figure 5.

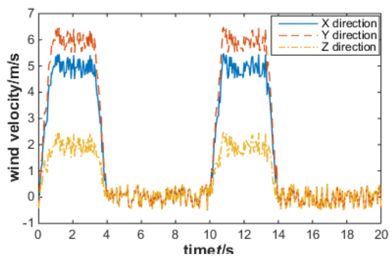

Fig. 5. Wind speed along X, Y, Z direction

Table 1 simulation parameter table

simulation parameter	numerical value	simulation parameter	numerical value
Elastic modulus of the cable：E/Gpa	100	Cable damping coefficient C/N/(mm/s)	0.2
Cable cross-sectional area：A/mm^2	0.13	Moving platform quality：m_B/Kg	1.2
A_i Distribution circle radius r_A/m	0.52	B_i Distribution circle radius r_A/m	0.25
$\boldsymbol{A}_i$ Distribution angle α_A/°	60	B_i Distribution angle α_A/°	60
The distance between support ring and O_A:H$_1$	0.07	The distance between platform surface and O_B:H$_2$	0.03
X direction of moving platform: I_X/ Kgm^2	0.81	The inertia of moving platform Y direction: I_Y/ Kgm^2	0.81
Z direction of moving platform: I_Z/ Kgm^2	1.57	Quality of platform: m_b/Kg	1.2
Air density: ρ/Kg/m^3	1.29	Resistance coefficient: C_d	0.45
Lift coefficient: C_l	0.05	Maximum cross section area of moving platform: S/m^2	0.16

A. *Cable length and cable tension calculation under ideal condition*

Ideally the cable only steady-state winding movement without slight vibration. The compound movement of flying cable driven parallel robot is shown in Figure 6 (a) with motion time T=10s. The four-rotor UAV moves in a straight line in {G}, the starting point for the [-20, -30, 40]m, [40 20, 102.45]m end point, and the attitude angle [ϕ_b, θ_b, φ_b]=[0, 0, 0]°. The moving platform horizontal circular motion in {B}, radius 1m, the center [0, 0, 1]m in {A}. The four-rotor UAV space linear motion, while in {G} the trajectory of the moving platform for the final composite as shown in Figure 5 (b) space helix is shown, helix radius r=1m, angular velocity w=0.2πrad/s. Cable length calculation results as shown in Figure 6, we can see that the length of cable and cable tension are continuously changing with time, because the trajectory is a spiral line, so the length of cable and cable tension according to sine or cosine variation, indicating the cable length and cable tension calculation is correct.

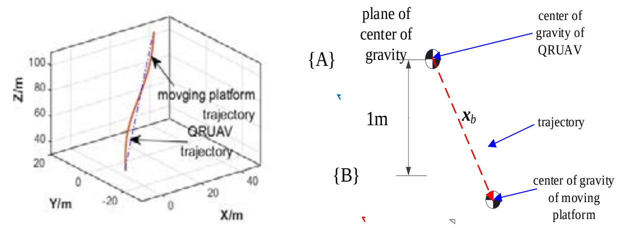

(a) Trajectories in the global frame system (b) Trajectories in the local frame system

Fig. 6. Moving platform trajectories

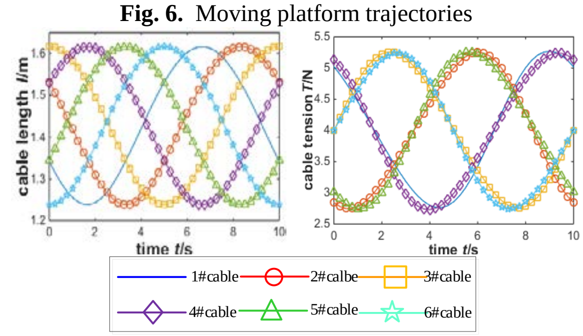

Fig. 7. Variation of cable length and cable tension in compound trajectory

B. *Analysis of Cable Length and Cable tension under Non -ideal Conditions*

Under the non-ideal condition, the cable has both steady state motion and small amplitude vibration. As shown in Figure 7, the four-rotor UAV hovering at the fixed point [50, 50, 100]m, the moving platform performs horizontal circle motion in {B}, the radius is r=1m, the center of the center frames in {A} is [0, 0, 1]m. Taking the trajectory under ideal condition as the desired trajectory (ET), it is a horizontal circle with height of 99m, and the trajectory of (ET+SV) under the condition of a desired trajectory. In order to facilitate the study of cable length and cable tension, 1# cable is taken as the research object. As shown in Figure 8, when the ideal condition is, the cable has no small amplitude vibration, and the long curve of the 1# cable is smooth and continuous. In the case of non-ideal condition, the cable has small amplitude vibration, the long curve of 1# cable is not smooth and continuous, and the cable length curve in ideal condition is small amplitude. Under the two conditions, the variation of cable length is the same, which are short→long → short. When the length of the cable increases, the angle between the cable pulling force and the vertical direction increases, and the cable tension must be increased to balance the gravity of the moving platform; otherwise, the cable tension decreases. Therefore, the cable tension curves of 1# cable in Fig. 9 vary according to the law, i.e. small→ large → small, which further proves the correctness of the cable tension solving algorithm. Figure 10 shows the ratio of cable tension increment to cable tension of 1# cable when small amplitude vibration is δ_{SV}, and defines $\delta_{SV}=\Delta T_1/ T_1\times100\%$. The maximum value of δ_{SV} is 12.47%, which is considerable.

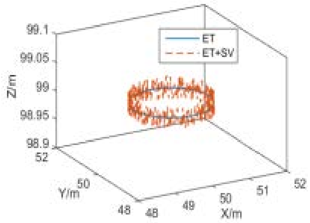

Fig. 8.
Expected trajectories and superimposed trajectories

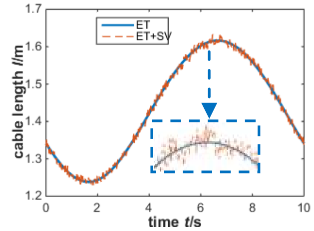

Fig. 9.
The length when 1# cable is under non-ideal condition

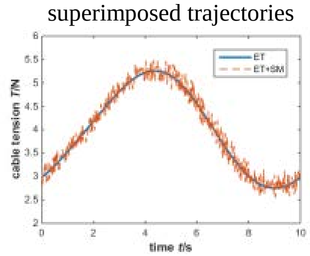

Fig. 10.
The force of 1# cable when Under non-idea condition

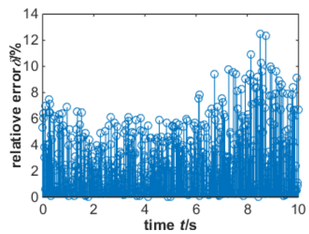

Fig. 11.
Tension ratio δ_{SV}

C. *Effect of four rotor unmanned aerial vehicle on cable tension*

To study the influence of four-rotor UAV motion on cable tension, the moving platform firstly stays in the local frame system, $[\phi_b, \theta_b, \varphi_b]=[0, 0, 0]°$. The spiral motion of four-rotor UAV is shown in Figure 12 with the start point is [0, 0, 1]m and end point [20, 20, 21]m, radius r=20m, Z direction speed V_Z=1m/s, movement time T=20s. During the movement of the four-rotor UAV, the roll angle ϕ_a=0°, the yaw angle φ_{a}=0°, while the pitch angle θ_a changes is shown in FIG. 13. Taking into account two conditions: one is condition A (considering the four-rotor UAV motion), the other one is condition B (without considering four-rotor UAV motion). Tensions of 1 # cable that referred to as T_A and T_B are calculated under two conditions respectively. The results shown in Figure 14, where you can find that the state of the cable A is seen to be larger than that of the cable B because of the speed and acceleration caused by the movement of the four-rotor, resulting in a $\boldsymbol{D}_B$ term. According to (27), (36) and (39), the upper and lower limits of tension T increases with the quad-rotor UAV mobility increases. Therefore, in order to ensure the normal output of the motor driving force, the four-rotor UAV should be kept as smooth as possible. The relative error of cable tension is defined as $\delta_{AB}=|T_A-T_B|/ T_A\times100\%$, and the maximum relative error of cable tension is 6.34%. It shows that the movement of four-rotor UAV has obviously influence on the cable tension solution.

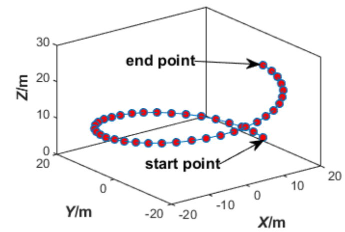

Fig. 12.
Four-rotor UAV trajectory

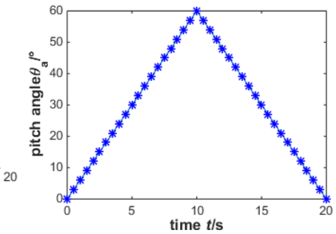

Fig. 13.
Changes of pitch angle θ_a

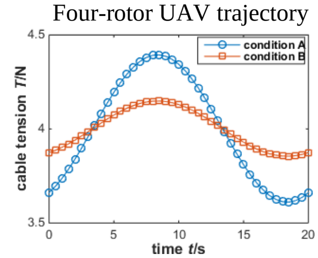

Fig. 14.
cable tension

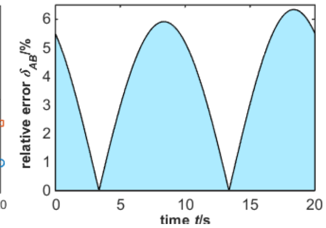

Fig. 15.
Relative error δ_{AB} of 1 # cable tension in two conditions

VII. Conclusion

(1) In this paper, the dynamic model of the flying cabled parallel robot is established. The cable's flexibility and external wind disturbance lead to the dynamic coupling between the two subsystems of the four-rotor unmanned aerial vehicle and the cabled parallel robot. Kinetic coupling can be described by decomposing the cable movement into steady-state winding movement and small-amplitude vibration.

(2) The slight vibration of cable will cause the increment of cable tension ΔT on the basis of the cable tension T of the steady-state retraction movement. According to the finite element method, ΔT can be solved by the spatial dispersion of the cable. The ratio of ΔT to T is up to 12.47%, which will significantly affect the accuracy of the cable T's solution. Therefore, when the force control is carried out, the vibration of the cable must be fully considered.

(3) In solving the cable tension T, the basic movement of the four-rotor unmanned aerial vehicle can be regarded as external interference $\boldsymbol{D}_B$. Four-rotor UAV movement of the higher mobility, then the upper and lower cable T range range. In order to ensure that the cable tension is within the feasible range, the stability of the four-rotor UAV should be ensured as much as possible.

References

[1] BERTI A, MERLET J P, CARRICATO M. solving the direct geometrico-static problem of underconstrained cable-driven parallel robots by interval analysis[J]. International Journal of Robotics Research, 2016, 35(6):723-739.

[2] LUCASSEN L R, STERK F J. Dynamic stability analysis of a hovering helicopter with a sling load[J]. Journal of the American Helicopter Society, 1965, 10: 6–12.

[3] NONNENMACHER D, KIM H, GÖTZ J, et al. System architecture of HALAS—a helicopter slung load stabilisation and positioning system[J]. CEAS Aeronautical Journal, 2013, 5(2): 127-143.

[4] Kim H M, NONNENMACHER D, GÖTZ J, et al. Initial flight tests of an automatic slung load control system for the ACT/FHS[J]. CEAS Aeronautical Journal, 2016, 7(2):209-224.

[5] NONNENMACHER D, JONES M. Handling qualities evaluation of an automatic slung load stabilization system for rescue hoist operations[J]. CEAS Aeronautical Journal, 2016, 7(4):587-606.

[6] ADAMS C, POTTER J, SINGHOSE W. Input-shaping and model-following control of a helicopter carrying a suspended load [J]. Journal of Guidance, Control, and Dynamics. 2015, (38)1: 94-105.
[7] OH S-R, PATHAK K, AGRAWAL S K, et al. Approaches for a tether-guided landing of an autonomous helicopter [J]. IEEE Transactions on Robotics. 2006, (22)3: 536-544.
[8] LIU Xin, QIU Yuanying, SHENG Ying. Proofs of existence conditions for workspaces of cable-driven parallel robots and a uniform solution strategy for the workspaces[J]. 2010, 46(7):27-34.
[9] LIU Xiongwei, ZHENG Yaqing. Kinematic analysis of a 6-dof cable-driven parallel kinematic manipulator[J]. Chinese Journal of Mechanical Engineering, 2002, 38(Suppl.): 16-20.
[10] Diao X, Ma O. Vibration analysis of cable-driven parallel manipulators[J]. Multibody System Dynamics, 2009, 21(4):347-360.
[11] Liu Z, Tang X, Shao Z, et al. Research on longitudinal vibration characteristic of the six-cable-driven parallel manipulator in FAST[J]. Advances in Mechanical Engineering, 2013(5): 547416-547416.
[12] Tang X, Liu Z, Shao Z, et al. Self-excited vibration analysis for the feed support system in FAST[J]. International Journal of Advanced Robotic Systems, 2014, 11(1):1-13.
[13] DU J, BAO H, CUI C, et al. Dynamic analysis of cable-driven parallel manipulators with time-varying cable lengths[J]. Finite Elements in Analysis & Design, 2012, 48(1):1392-1399.
[14] DU J, DING W, BAO H. Cable Vibration Analysis for Large Workspace Cable-Driven Parallel Manipulators[A]. BRUCKMANN T POTT A. Cable-Driven Parallel Robots[C]. Berlin: Springer, 2013:437-449.
[15] SU Yu, QIU Yuanying, WEI Huiling. Dyanmic modeling and tension optimal distribution of cable-driven parallel robots considering cable mass and inertia force effects[J]. ENGINEERING MECHANICS, 2016, 33(11):231-239.
[16] Tran N K, Bulka E, Nahon M. Four-rotor control in a wind field[C]// International Conference on Unmanned Aircraft Systems. IEEE, 2015:320-328.

Qin Wang was born on Nov. 3, 1981**.** He received the master degree in mechanical manufacturing and automation from Xi'an Technological University of China. Currently, he is a lecturer at Xi'an Technological University, China. His major research interests include specialized robot and wheeled robots.

Hua Chen was born on Jan. 16, 1962**.** He received the PhD degree in Mechanical Manufacturing and Automation from Xi'an Jiao Tong University of China. Currently, he is a professor and tutor of postgraduate candidates at Xi'an Technological University, China. His major research interests include Numerical integrated manufacturing technology and Intelligent Manufacturing Technology.

Yu Su was born on Jul. 18, 1982**.** He received the PhD degree in mechatronic engineering from Xidian University of China. Currently, he is a lecturer at Xi'an Technological University, China. His major research interests include specialized robot and cable driven parallel robots.